Storms, E. and B. Scanlan. *Detection of Radiation Emitted from LENR*. in *ICCF-14 International Conference on Condensed Matter Nuclear Science*. 2008. Washington, DC.

Detection of Radiation Emitted from LENR

Edmund Storms and Brian Scanlan
Kiva Labs,
Santa Fe, NM and Greenwich, CT

ABSTRACT

A study was made to detect X-radiation and energetic particle emission from nuclear reactions that may be initiated during low-voltage gas discharge in deuterium. Evidence is presented for X-radiation having an energy nearly equal to the voltage applied to the discharge and energetic particle emission similar to deuterons having energy with peaks between 0.5 and 3 MeV. A study of radiation emitted from materials exposed to deuterium gas is underway.

I. INTRODUCTION

Emission of radiation is characteristic of nuclear reactions. Such radiation is required to carry away momentum and energy from the reaction and deposit it as heat in the environment. In contrast, the nuclear reactions associated with cold fusion appear to produce less radiation than expected when detection is attempted outside of the apparatus. This unexpected behavior has encouraged a search for low-energy radiation within the device. This search is important because detected radiation clearly shows that nuclear reactions are occurring and provides information about the process. Consequently, such observations are far more supportive of a nuclear reaction than the conventional measurement of heat.

In addition to heat energy, cold fusion is found to produce helium[1-12] and occasionally tritium[13-21]. The helium is expected to originate as energetic alpha particles and the tritium as energetic tritons. A search for such energetic particles has been undertaken by other workers using CR-39 as the detector.[22-26] However, energetic particles can also be detected using a silicon barrier detector (SBD), from which their energy can be obtained, or by use of a Geiger-Mueller (GM) counter, using absorbers to determine their energy. These methods are used in this study to measure the energy of the detected radiation. This paper further describes studies reported previously. [27,28]

Two methods to initiate a fusion reaction have been explored. First, a discharge has been studied in low-pressure D_2 gas using various kinds of cathode materials. Second, fine powders of materials containing palladium have been exposed to pressurized D_2 gas. Both the SBD and GM detectors were used in the former study while only the SBD was used in the latter work.

II. EXPERIMENTAL

II.1. Gas Discharge

The gas discharge cell is shown in Fig. 1. The cathode is a water-cooled thin sheet of various metals including, Al, Cu, Pd, Pd+Pt, Pt Ti, bronze, brass, or stainless steel. The cathode is surrounded by a shroud consisting of various insulators including Teflon, Lavite, Al_2O_3 or BN

in order to force the discharge to occur within a well defined region of the metal surface. The anode is either a Pd or W rod located so as not to block the view of the cathode by the detectors. The system is evacuated using a turbomolecular pump capable of reaching pressures less than $1x10^{-7}$ Torr. After evacuation, the system is filled with deuterium gas (99.95% D + 0.05% H) to a pressure between 10 and 40 Torr, depending on the nature of the study. Gases consisting of N_2, O_2, Ar, H_2, H_2O, or D_2O are used either alone or mixed with D_2. A DC voltage between 500 V and 900 V is applied at a current between 0.05 A and 0.3 A, using current control. The various measurements are recorded using Labview (National Instruments) and Maestro (Ortec) programs with an iMAC computer running both Windows XP and OS10.5.4.

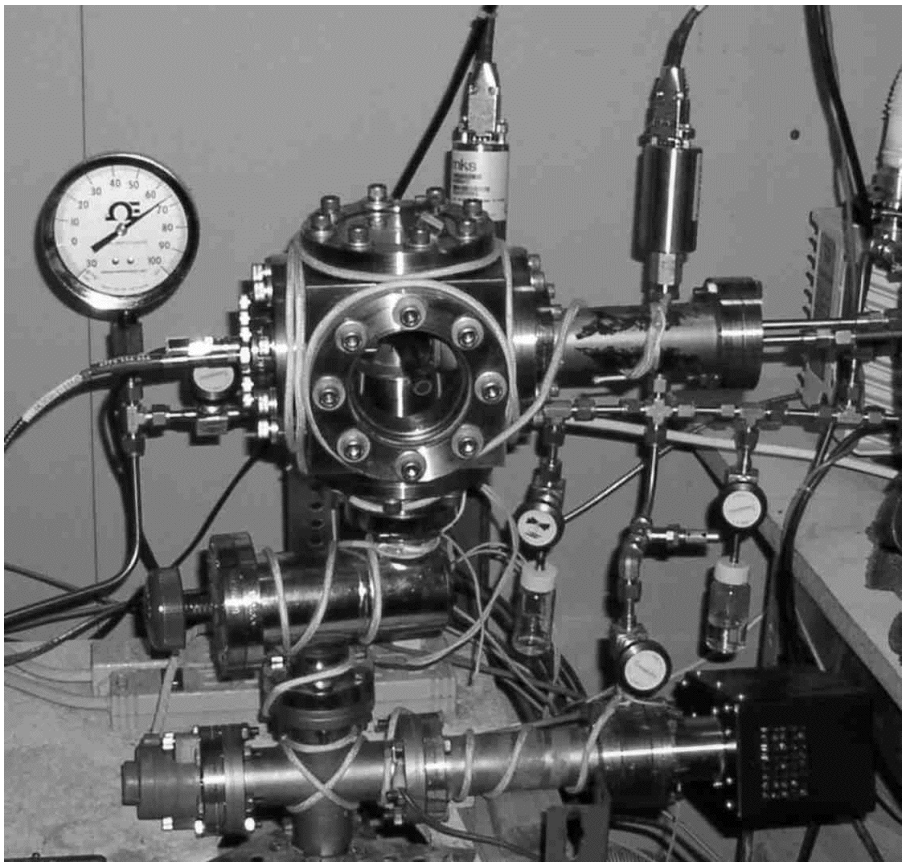

FIGURE 1. Picture of the gas discharge apparatus. The detectors are located on the left and the water cooled cathode is on the right. H_2O or D_2O vapor is supplied from small glass containers of the liquid as seen on the right.

The cathode surface is viewed by either a SBD, a GM, or both at the same time. Various SBD made by Ortec are used. Calibration of the SBD is done using Po^{210} in vacuum. The shape of the peak in vacuum (Fig.2) has a Gaussian relationship on the high-energy side but has slight broadening on the low-energy side caused by self-adsorption. Most of the peaks attributed to charged particles found in this study could be fit by a similar Gaussian equation. A study of energy vs. distance between the source and detector in air shows that the relationship between BIN number and energy is linear, as can be seen in Fig. 3. The BIN number was calibrated at lower energy by using a source of pulses (Ortec 419) having a linear relationship to energy that were fed into the preamp at the same location as the pulses from the SBD. An example of a peak

produced by these pulses is shown in Fig. 2. However, the apparent energy has to be modified because the SBD is covered by a thin aluminum light shield that removes some energy, depending on the kind of particle passing through it. The various corrections are listed in Table 1 for energy near 1 MeV based on the ASTAR tables. Because the kind of particle is not known initially, the apparent energies noted on the figures are the measured value without a correction for the light shield. The values are only used to compare the relative effects of absorbers and applied voltage. Once the particles have been identified later in the paper, actually energy will be assigned to each peak.

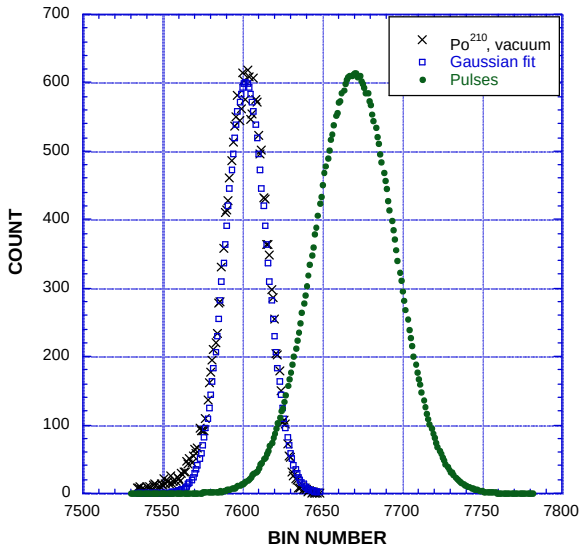

FIGURE 2. Count vs BIN number for Po^{210} compared to a Gaussian fit and output of the pulser.

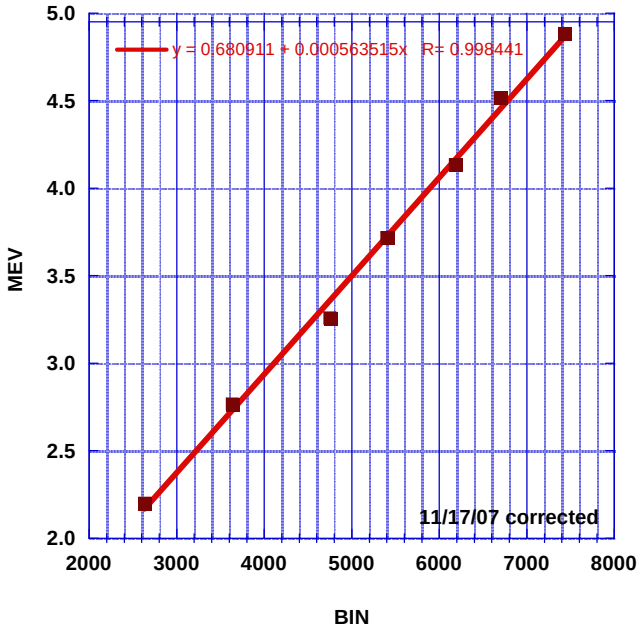

FIGURE 3. Typical calibration using air to change the energy of Po^{210}.

A system of moveable absorbers allows various thickness of Mylar, aluminum or copper to be imposed between the cathode and detectors. As many as three absorbers could be imposed during the same run in front of either the GM or the SBD. One of these absorbers is always a thickness of copper sufficient to completely stop the radiation. Only counts that are completely stopped by this absorber are accepted as being caused by actual radiation, in contrast to being caused by electrical noise in the counting circuit. Such noise was frequently generated by the electrical discharge when conditions had not been properly adjusted.

Two different GM tubes made by LND were used, one with a 2.5 mg/cm^2 window and the other with a 0.3 mg/cm^2 window. Because of its reduced absorption, the thin-window tube had a higher counting rate in spite of having a window only 1.5 mm in diameter compared to the 9 mm diameter of the other tube.

TABLE 1
Change in energy produced by passing 1 MeV particles
through absorbers based on ASTAR tables

	1.2 μm Aluminum	2.0 μm Mylar	3.0 μm Mylar
Alpha, MeV	0.39	0.54	0.81
Proton, MeV	0.075	0.095	0.14
Thickness, g/cm^2	0.000324	0.00028	0.00042

Calibration equation for SBD: MeV = 0.000657*BIN

III. RESULTS

III.1. Particle Measurement

Many peaks in the SBD spectrum were detected, some of which were clearly produced by electrical noise injected into the detection circuit by the discharge. Peaks that could be eliminated by imposing a thick absorber in front of the SBD are assumed to be caused by real particles. Further support for this conclusion is obtained when the intensity and energy are reduced by a thin absorber.

The sequence of the measurement is shown by the data number in each of the following figures. A few figures show the counting rate of a GM counter that detected the X-radiation emitted from the cathode along with the particles. The energy noted on the figures is uncorrected for the light shield. Therefore it can only be used to show relative changes in energy produced by the absorbers and voltage. The complete data set is listed in Table 2 along with corrected energies based on the particles being alpha or protons. A conclusion about the kind and energy of the particles is saved for the discussion section.

A gas mixture of approximately equal amounts of D_2 and D_2O produces the spectra shown in Figs. 7, 8, and 9. When 721 V is applied, a weak emission at 0.32 MeV is produced. Increasing the voltage to 771 V causes a peak to appear at 0.20 MeV, with an indication of a peak near 0.1 MeV that is partially overlapped by the noise region. A further increase to 800 V causes a peak at 0.26 MeV, with a decrease in intensity, and additional radiation near 0.1 MeV to form. Moving to Fig. 8, imposition of 3.0 μm of Mylar at 800 V reduced the peak at 0.26 MeV to 0.23 MeV without significantly changing the peak near 0.1 MeV. A thick copper absorber eliminated all peaks. When a 2.0 μm Mylar absorber is used instead of the 3.0 μm Mylar at 767 V, the peak shifts by 0.02 MeV showing the effect of 1.0 μm of Mylar, as seen in Fig. 9. Again, a thick absorber eliminates all peaks except for the noise below about BIN = 150.

TABLE 2

Summary of all data

Date	Absorber	Applied volt	BIN	Intensity for 1 min	Measured, MeV	Alpha, MeV	Proton, MeV	Gas composition
11/28/07	1.2 μm Al	823	640	65	0.42	0.81	0.50	D_2+D_2O
	1.2 μm Al	823	1430	5	0.94	1.33	1.01	D_2+D_2O
12/7/07	1.2 μm Al	760	300	4125	0.20	0.59	0.27	D_2+H_2O
	1.2 μm Al	760	680	400	0.45	0.84	0.52	D_2+H_2O
	1.2 μm Al	760	1100	50	0.72	1.11	0.80	D_2+H_2O
	1.2 μm Al	760	1500	25	0.99	1.38	1.06	D_2+H_2O
12/10/07	1.2 μm Al	721	480	10	0.32	0.71	0.39	D_2+D_2O
	1.2 μm Al	771	300	25	0.20	0.59	0.27	D_2+D_2O
	1.2 μm Al	800	400	12	0.26	0.65	0.34	D_2+D_2O
	1.2 μm Al+3.0 μm Mylar	801	350	25	0.23	1.43	0.44	D_2+D_2O
	1.2 μm Al+3.0 μm Mylar	764	430	10	0.28	1.48	0.50	D_2+D_2O
	1.2 μm Al+2.0 μm Mylar	767	460	12	0.30	1.23	0.47	D_2+D_2O
12/11/07	1.2 μm Al	767	340	29	0.22	0.61	0.30	D_2+D_2O
	1.2 μm Al	777	350	30	0.23	0.62	0.30	D_2+D_2O
	1.2 μm Al	788	390	50	0.26	0.65	0.33	D_2+D_2O
	1.2 μm Al	791	420	152	0.28	0.67	0.35	D_2+D_2O
	1.2 μm Al	791	1100	10	0.72	0.86	1.53	D_2+D_2O
	2*1.2 μm Al	777	590	10	0.39	1.17	0.54	D_2+D_2O
	2*1.2 μm Al	781	none					D_2+D_2O
	1.2 μm Al+3.0 μm Mylar	786	520	20	0.34	1.54	0.56	D_2+D_2O
	1.2 μm Al+3.0 μm Mylar	766	350	10	0.23	1.43	0.44	D_2+D_2O
12/12/07	1.2 μm Al	671	350	10	0.23	0.62	0.30	H_2+D_2+H_2O
	1.2 μm Al	756	330	400	0.22	0.61	0.29	H_2+D_2+H_2O
	1.2 μm Al	756	750	30	0.49	0.88	0.57	H_2+D_2+H_2O
	1.2 μm Al	756	1160	5	0.76	1.15	0.84	H_2+D_2+H_2O
	1.2 μm Al+3.0 μm Mylar	785	300	2	0.20	1.40	0.41	H_2+D_2+H_2O
12/13/07	1.2 μm Al	739	280	550	0.18	0.57	0.26	H_2+H_2O
	1.2 μm Al	739	690	40	0.45	0.84	0.53	H_2+H_2O
	1.2 μm Al	739	1100	10	0.72	1.11	0.80	H_2+H_2O
	1.2 μm Al	739	1550	5	1.02	1.41	1.09	H_2+H_2O
	1.2 μm Al	773	440	900	0.29	0.68	0.36	H_2+H_2O
	1.2 μm Al	773	950	75	0.62	1.01	0.70	H_2+H_2O
	1.2 μm Al	773	1520	15	1.00	1.39	1.07	H_2+H_2O
	1.2 μm Al	773	2050	5	1.35	1.74	1.42	H_2+H_2O
	1.2 μm Al	794	540	450	0.35	0.74	0.43	H_2+H_2O
	1.2 μm Al	794	1170	45	0.77	1.16	0.84	H_2+H_2O
	1.2 μm Al	794	1820	7	1.20	1.59	1.27	H_2+H_2O

Date	Absorber	Voltage	BIN	Intensity	Measured, MeV	Alpha, MeV	Proton, MeV	Gas composition
	1.2 μm Al	794	2650	5	1.74	2.13	1.82	H_2+H_2O
	1.2 μm Al	794	3100	5	2.04	2.43	2.11	H_2+H_2O
	1.2 μm Al	794	3600	2	2.37	2.76	2.44	H_2+H_2O
	2*1.2 μm Al	774	500	6	0.33	1.11	0.48	H_2+H_2O
	2*1.2 μm Al	774	250	33	0.16	0.94	0.31	H_2+H_2O
12/18/07	1.2 μm Al	748	290		0.19	0.58	0.27	D_2+D_2O
	1.2 μm Al	785	420	7	0.28	0.67	0.35	D_2+D_2O
	1.2 μm Al	815	550	6	0.36	0.75	0.44	D_2+D_2O
	1.2 μm Al	845	730	30	0.48	0.87	0.55	D_2+D_2O

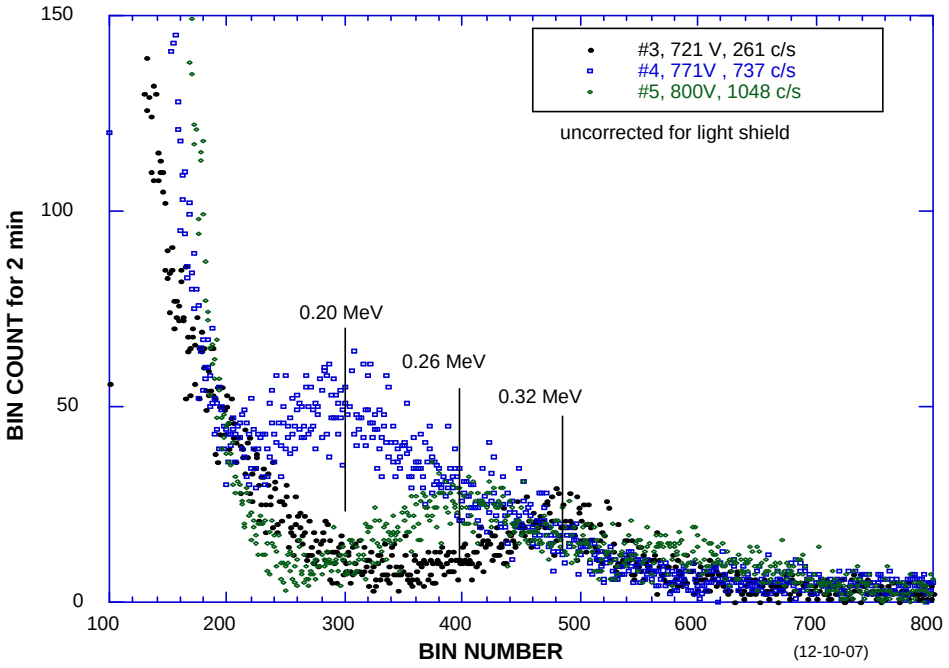

FIGURE 7. Spectrum produced using a Cu cathode, Al_2O_3 shroud, and a gas containing D_2 and D_2O at about 18 Torr. The count rate of the GM counter has a linear relationship to voltage and, in this case, extrapolates to zero at 695 V.

The next day, the system was opened to air and new absorbers were installed. The gas is again a mixture of D_2+D_2O. A clear peak can be seen in Fig. 10 at 0.28 MeV for 791 V and a smaller peak at 0.72 MeV. An energy of 0.34 MeV is produced at 786 V when 3.0 μm Mylar is inserted and this decreases to 0.39 MeV for 777 V when extra 1.2 μm Al is imposed. Imposition of 1.3 mm Cu stops all radiation below BIN=200, shown in Figs. 11 and 12. Counts below BIN=200 are assumed to result mainly from noise, although some counts in this region are removed by the thick absorber. Use of 3.0 μm Mylar at 766 V produces a peak at 0.23 MeV similar to the peak produced without Mylar at 777 V, as shown in Fig. 12.

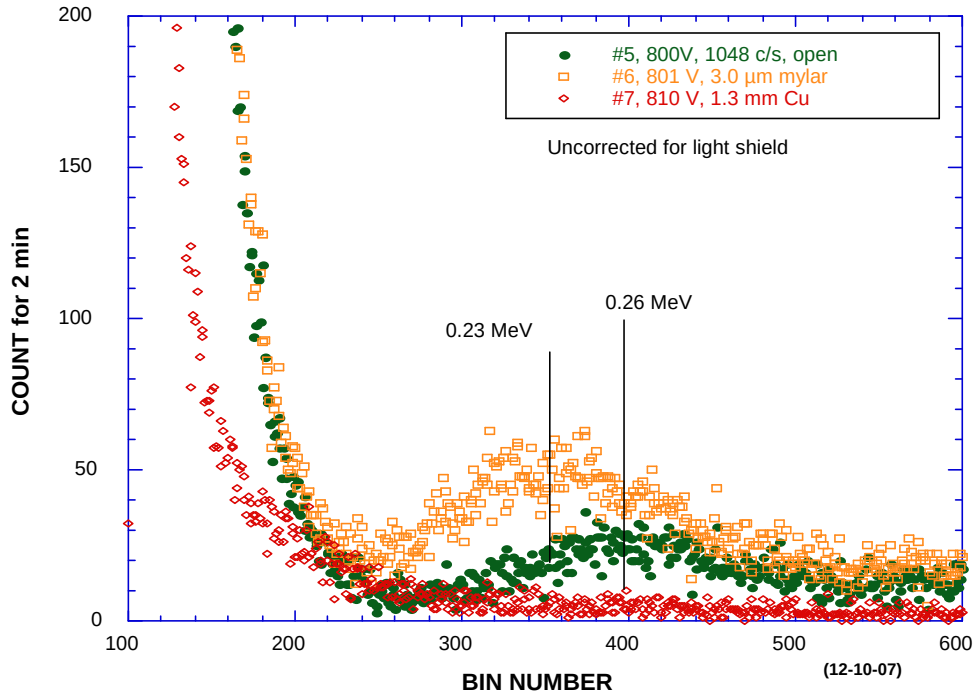

FIGURE 8. Spectrum produced using a Cu cathode, Al_2O_3 shroud, and a gas containing D_2 and D_2O at about 18 Torr.

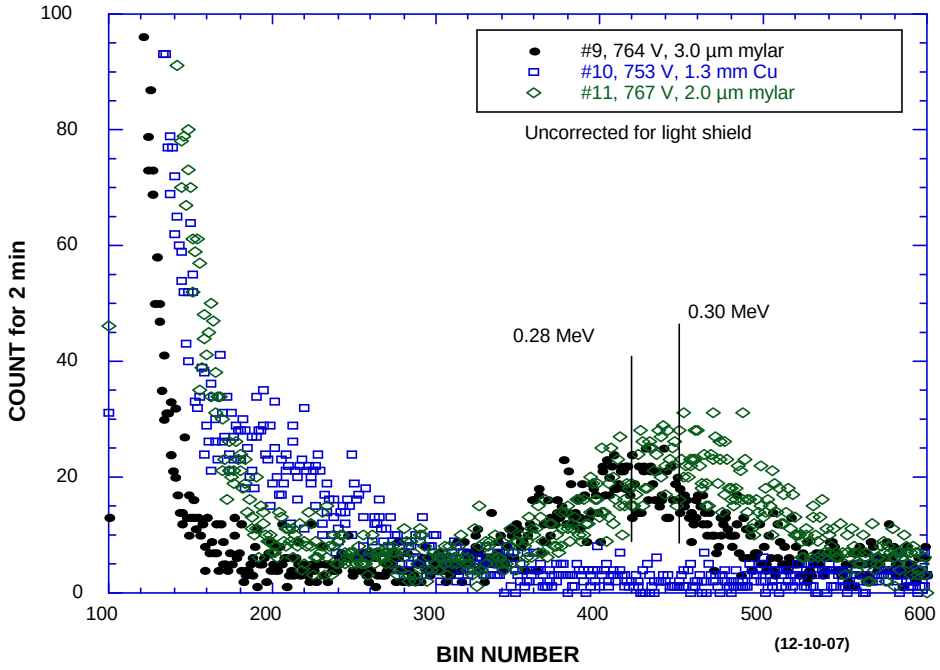

FIGURE 9. Spectrum produced using a Cu cathode, Al_2O_3 shroud, and a gas containing D_2 and D_2O at about 18 Torr.

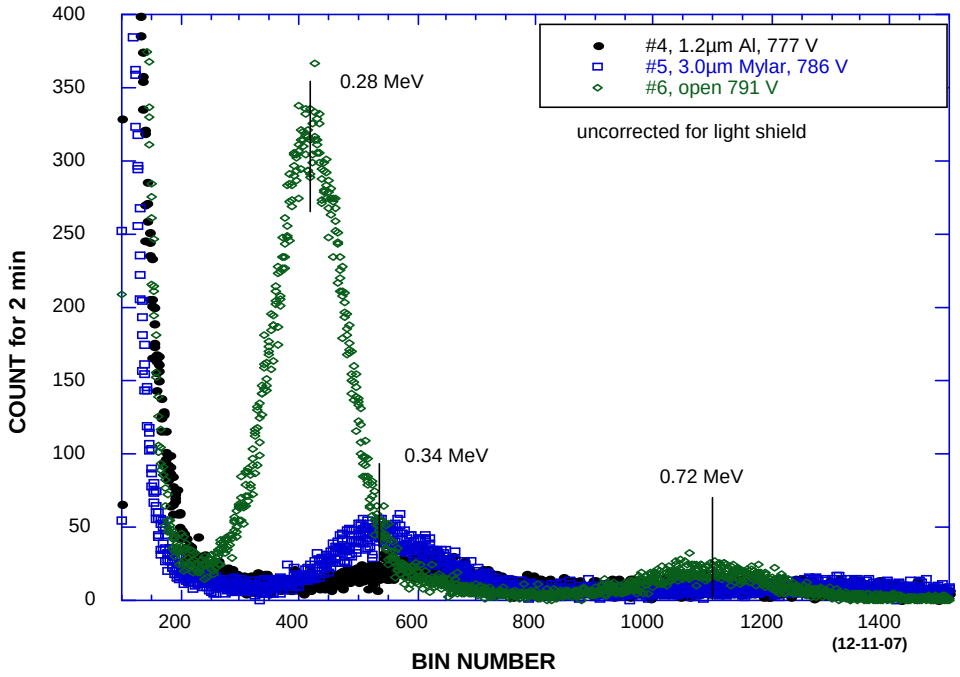

FIGURE 10. Spectrum produced using a Cu cathode, Al_2O_3 shroud, and a gas containing D_2 and D_2O at about 23 Torr.

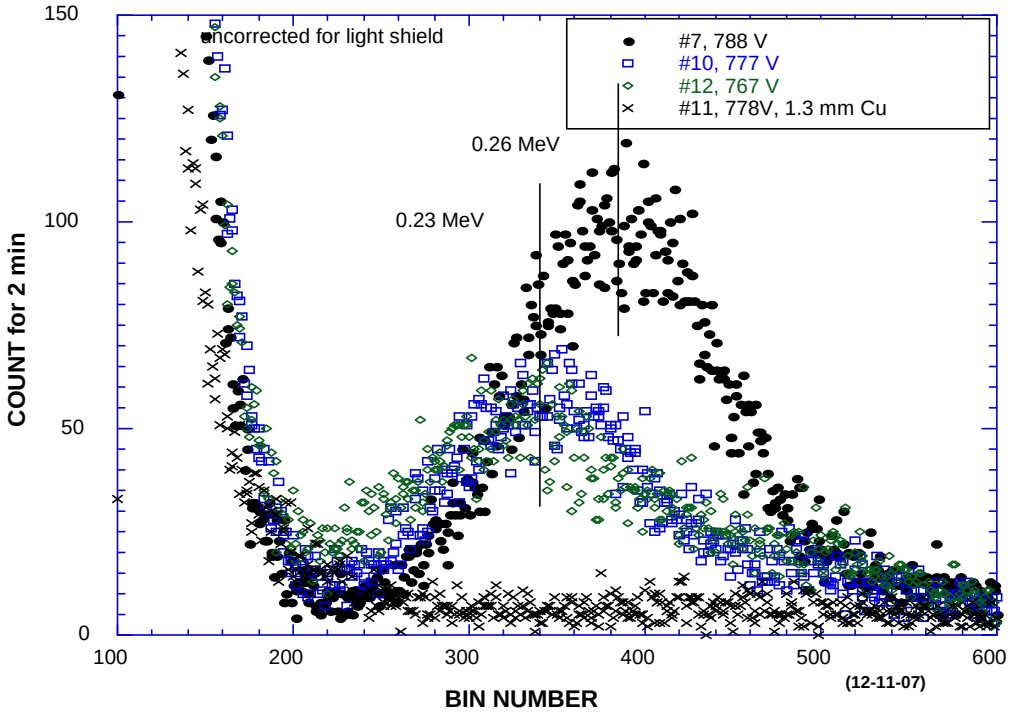

FIGURE 11. Spectrum produced using a Cu cathode, Al_2O_3 shroud, and a gas containing D_2 and D_2O at about 23 Torr.

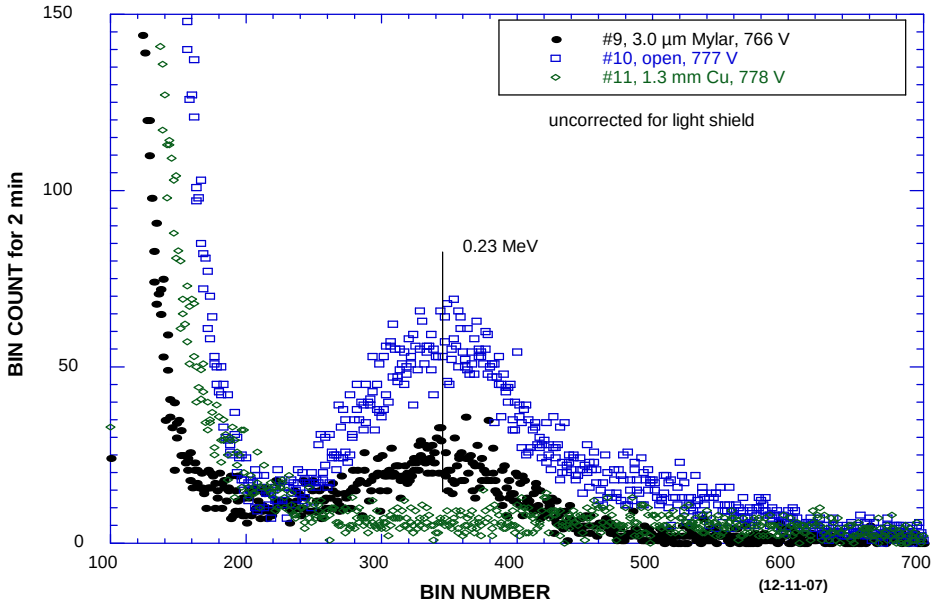

FIGURE 12. Spectrum produced using a Cu cathode, Al_2O_3 shroud, and a gas containing $12.0D_2$ and $11.4D_2O$ at about 23 Torr.

The gas mixture was changed to D_2, H_2 and H_2O, which causes the intensity of the radiation to increase. Imposition of 3 µm Mylar shifts the peaks near 0.1 MeV and 0.22 MeV off scale and shifts the peak at 0.49 MeV to 0.20 MeV, as shown in Fig. 13.

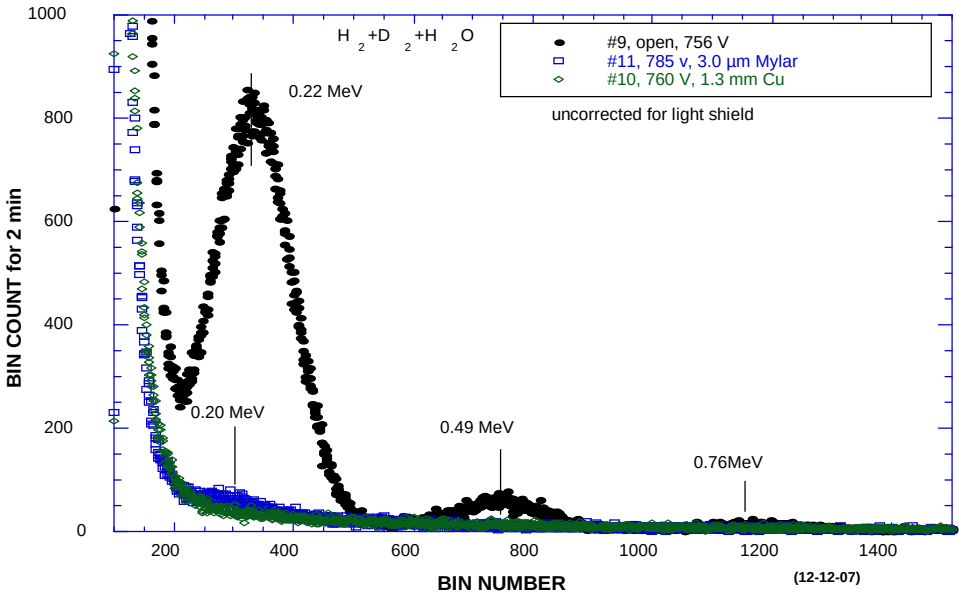

FIGURE 13. Spectrum produced using a Cu cathode, Al_2O_3 shroud, and a gas mixture of $2.8D_2$, $8.9H_2$, and $11.0H_2O$, with a total pressure of about 23 Torr.

When most D_2 is removed from the gas by using a mixture of H_2+H_2O, radiation intensity remains high and the spectrum becomes more complex, with additional peaks as shown in Figs.

14 and 15. The full spectrum of run #12 is shown in Fig. 16. Peaks at 2.37 MeV are visible. The energy of the peaks increases as applied voltage is increased. In contrast, no peaks fall on scale when the voltage is as low as 706 V.

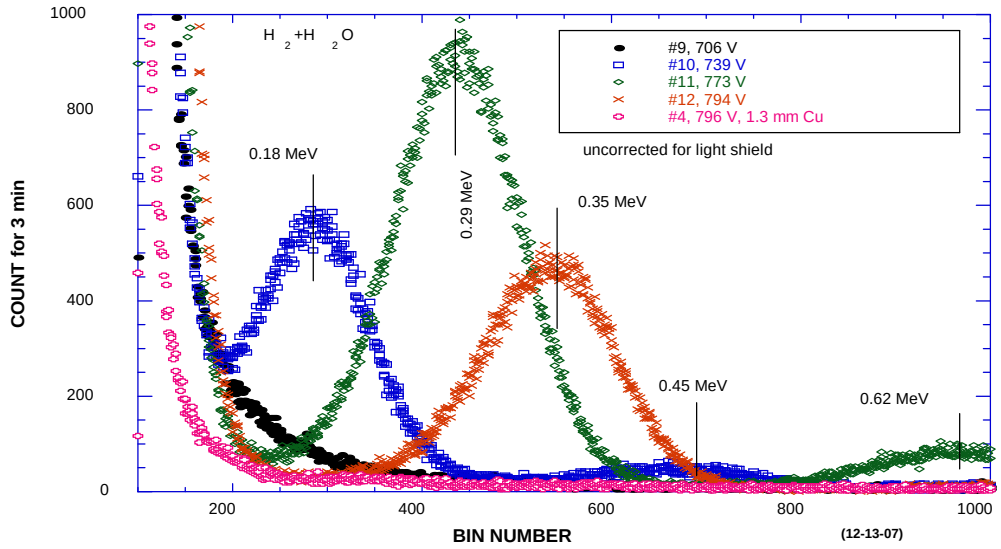

FIGURE 14. Spectrum produced using a Cu cathode, Al_2O_3 shroud, and a gas mixture of 8.5H_2 and 10.6H_2O with a total pressure of about 19 Torr. A small amount of D_2 is present in the gas, caused by release of absorbed gas after previous exposure to deuterium.

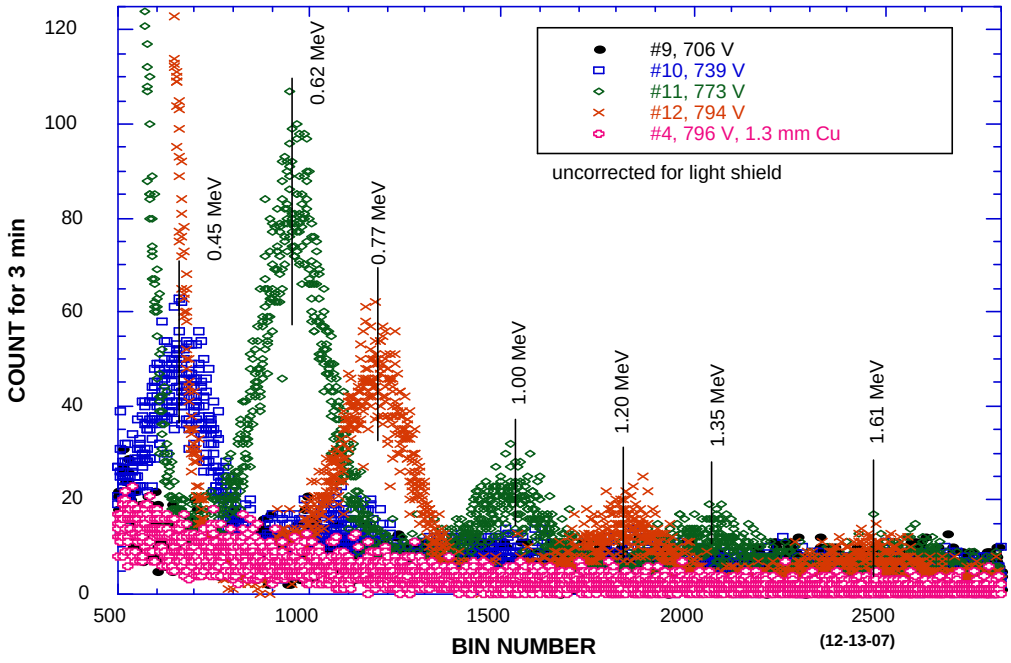

FIGURE 15. Spectrums shown in Fig. 14 from 500 to 2700 BIN number.

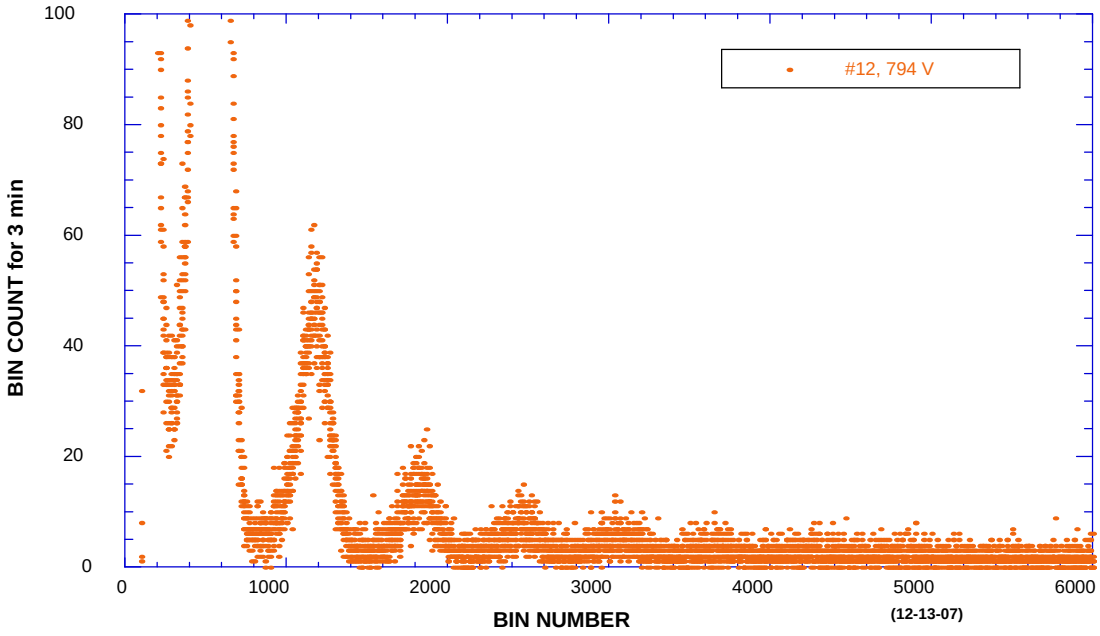

FIGURE 16. Full spectrum of run #12 from Figs. 14 and 15.

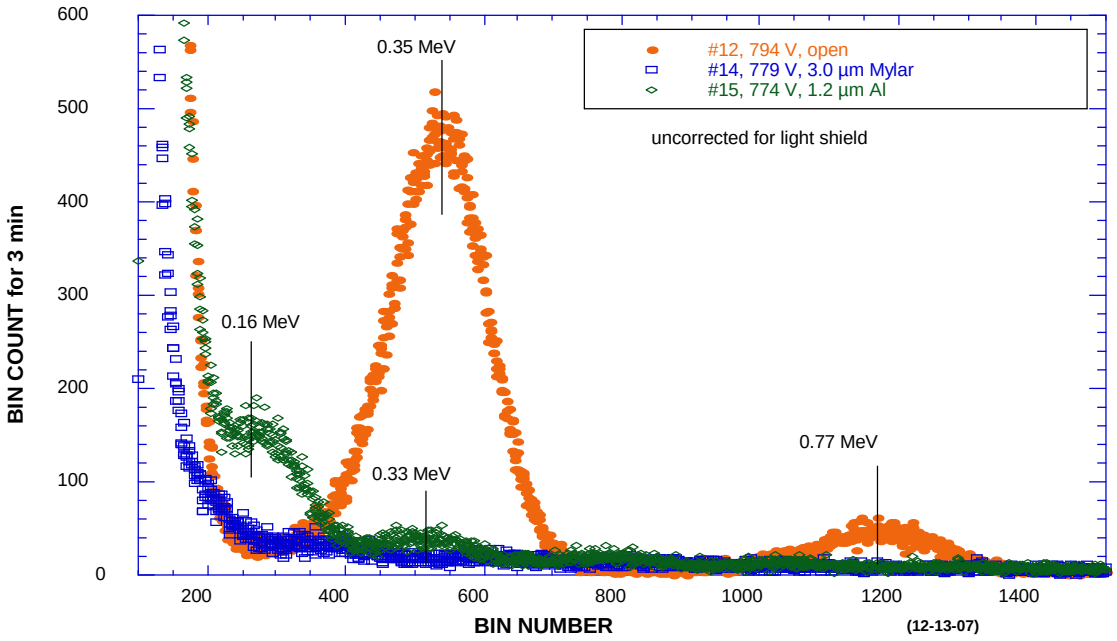

FIGURE 17. Effect of interposing 3.0 µm Mylar or 1.2 µm Al following run #12.

Imposition of 3.0 µm Mylar along with a reduction in voltage to 779 V eliminated all peaks. In contrast, 1.2 µm Al imposed at 774 V produced peaks at 0.16 MeV and 0.33 MeV.

II.2. Gas Loading

Gas loading involves exposure of special materials to D_2 gas, as pioneered by Arata and Zhang[29], and Case[30]. This method has been found to produce helium and excess heat when the proper materials are used. This method has several advantages over gas discharge for measuring radiation. For example, the background electrical noise generated by a discharge is not present, thereby allowing much lower energies and smaller fluxes of radiation to be measured. Absence of a light shield, as required during gas discharge, reduces the uncertainty in the measured energy. In addition, much greater control over the nature of the active material can be achieved.

Samples of various powdered materials are placed on a stage, shown in Fig. 18, that is within about 4 mm of a SBD, shown in Fig. 19. This stage is heated by passing current through an enclosed resistor and its temperature is measured using a type-K thermocouple located at the sample. An absorber made of 0.5 mm thick copper can be imposed between the SBD and the sample by moving an exterior rod. The assembly can be evacuated to less than $5x10^{-7}$ Torr and can be filled with purified D_2 or H_2 at pressures up to 100 psi.

A vacuum/hydrogen furnace used to purify the samples is shown in Fig. 20. This system can be evacuated to less than $5x10^{-7}$ Torr, pressurized with H_2 or D_2 up to 100 psi, and heated up to 500°C. The sample is contained in a thin Al cup that allows the powder to be removed and weighted after each treatment. The overall system is shown in Fig. 21.

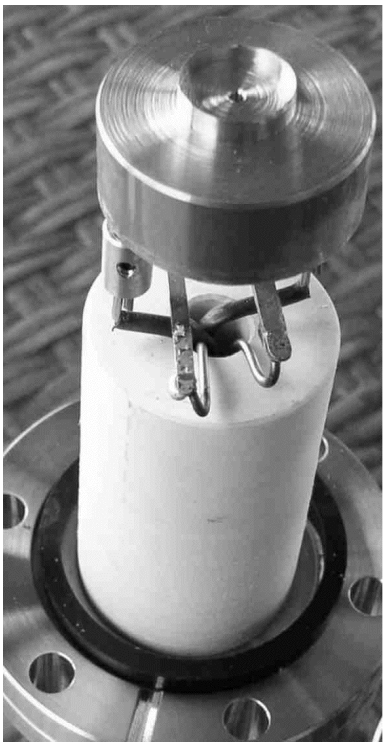

FIGURE 18. A heated platen holds the powdered sample in the cup, into which a thermocouple is inserted. The white material is Teflon that is used to stabilize the source and to decrease gas volume.

FIGURE 19. Holder for the SBD. When assembled, the active area of the SBD is located about 4 mm directly above the cup in the heated platen shown in Fig. 18. The massive copper helps keep the SBD cool when the sample is heated.

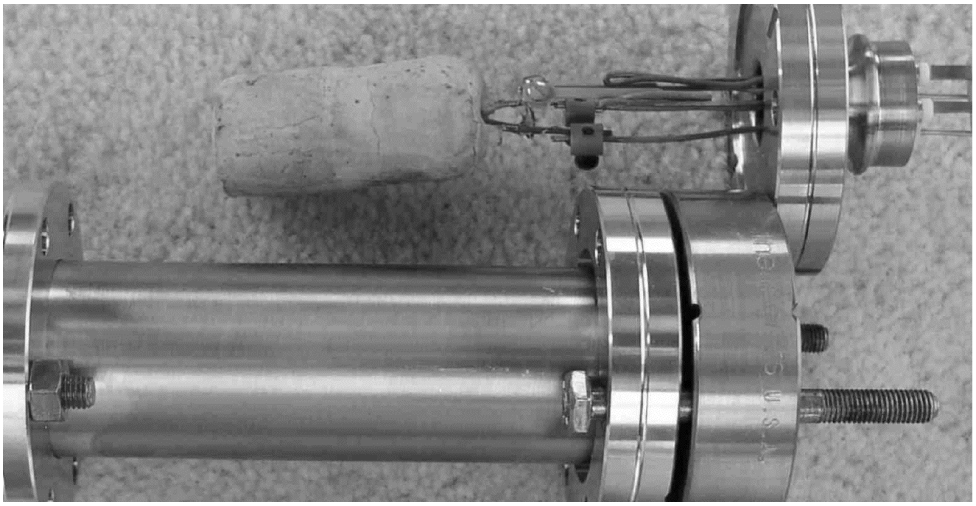

FIGURE. 20. Hydrogen furnace. The furnace consists of a brass tube wrapped with resistance wire imbedded in ceramic insulation. A thermocouple is inserted in the bottom.

A sample consisting of finely powdered (~2 μm particles) mixture of SiO_2, TiO_2, CaO, Al_2O_3, and CeO_2 is mixed with a solution of $Pd(NO_3)_2$ in water. The liquid is evaporated to dryness at 120°C in air. After purification with D_2 using the hydrogen furnace described above, the material is examined using the SBD. Fig. 22 shows the spectrum obtained with and without

the absorber in place. An identical spectrum is found using a sample of the same material, but without added Pd or exposure to D_2. A sample of powdered KOH is also examined and found to produce the same spectrum as the mixed oxides.

FIGURE 21. Overview of vacuum system and gas handling system. The detector assembly is on the left and the hydrogen furnace assembly is on the right of the red vacuum valves. Vacuum is measured using a nude ion gauge and a 0-100 Torr Baratron gauge. A RGA allows the gas composition to be determined. Gamma and neutron detectors are located nearby. A hydrogen gas-purifier is located in the rear.

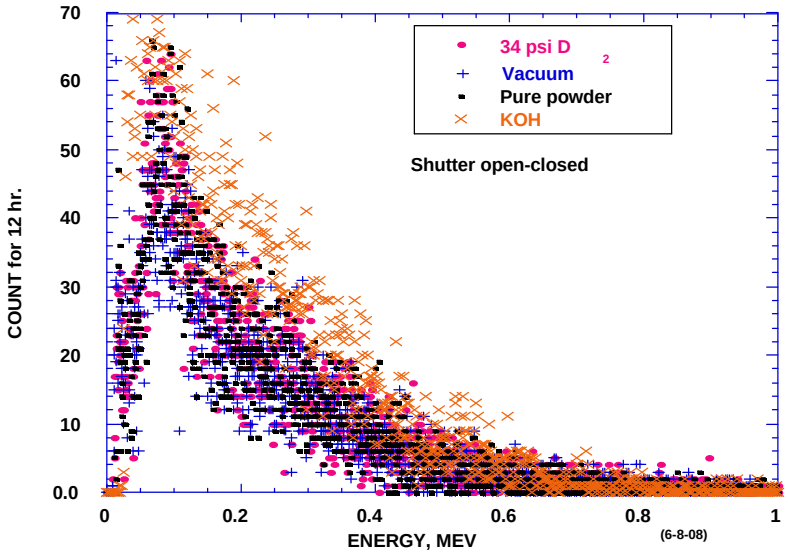

FIGURE 22. Difference between count for 12 hr with shutter open and closed using a sample of mixed oxides under various conditions. The powder was initially studied under 34 psi D_2 followed by vacuum. The pure power did not contain Pd nor was it exposed to D_2. The data are compared to the radiation from KOH (1.33 MeV beta from K^{40}) measured using the same apparatus.

III.3. Preparation and characterization of materials

The materials are made by evaporating at 120°C a dilute solution containing $PdCl_2$ or $Pd(NO_3)_2$ mixed with a suspension of a powder. In one case, the powder consists of a mixture of various oxides. The palladium compound in the powder is reduced to Pd metal by heating it in H_2/D_2 followed by pumping out the resulting reaction products. Once activated, the powder is heated in D_2 gas. In the process, weight is increased by absorbed or reacted deuterium. If all of the deuterium is present as β-PdD, the added weight should be proportional to the Pd content of the powder. If this proportionally is not observed, the deuterium is assumed to be absorbed on the oxide surface either as D_2 molecules or spill-over D+. By determining the weight increase of a sample containing no Pd, the amount of absorbed deuterium as D_2 can be determined because in the absence of a catalyst the D+ cannot form. This type of study was done using the materials listed in Table 3. The SiO_2 samples are made by evaporating a solution of $Pd(NO_3)_2$ with a colloidal suspension of SiO_2 in H_2O.

TABLE 3

Composition wt. % Pd wt% D_2 D/Pd

DESCRIPTION	Wt.% Pd	Wt. % D2	D/Pd	TREATMENT
SiO_2 (pure)	0.0	0.090	NA	40psi D_2
SiO_2#7c	0.23	0.030	6.9	40 psi D_2
SiO_2#9e	0.92	0.20	11.5	100 psi D_2
SiO_2#9d	0.92	0.24	13.8	80 psi D_2
SiO_2#10a	1.37	0.24	9.3	50 psi D_2
SiO_2#10b	1.37	0.31	12.0	30 psi D_2
Al_2O_3#1a	0.41	0.23	29.2	20 psi D_2
ZrO_2#1a	0.39	0.09	12.5	30 psi D_2

III.4 X-ray measurement

The X-ray measurements were described previously.[27,28] The radiation originates at the cathode, which acquires a very complex surface. Consequently, emission is probably not uniform. Use of absorbers allows the energy of the X-rays to be determined. Figure 23 compares the counting rate as a function of applied volt for when various absorbers are placed between the GM tube and a Mo cathode using a gas mixture of D_2O and D_2 at 22 Torr. No absorber is used periodically during the study and these results are combined and fit by the equation

$c/s = 0.002 * (V - 482)^3$, where V is the applied voltage.

The form of this equation was chosen because it fits well the relationship between absorption coefficient and X-ray energy as provided by NIST. The counting rate (c/s) obtained using this equation is divided into the measured counting rate for each absorber to calculate I/Io. An apparent absorption coefficient can be obtained using the equation

μ/ρ (cm^2/g) = - ln(I/Io)/t, where t is the absorber thickness in g/cm^2.

The calculated absorption coefficients for the aluminum absorbers are compared in Fig. 24 to the tabulated values provided by NIST. Apparently the X-ray energy is less than the applied voltage at low voltages, being about 400 eV when the applied voltage is 525 V. However, the X-ray energy and the applied voltage become equal as applied voltage is increased to about 600 V. The Mylar absorbers show results that are consistent with this behavior. Because the shape of the measured curve is very sensitive to the form of the equation used to calculate Io above 600 V, the effect of voltage on X-ray energy becomes increasingly uncertain at higher voltages. Nevertheless, as voltage is increased, the increased energy of the radiation allows more radiation to pass through the window of the GM tube resulting in an increasing counting rate when applied voltage is increased. The higher the oxygen content of the gas, the more rapidly the counting rate increases with applied voltage, as described previously.[27]

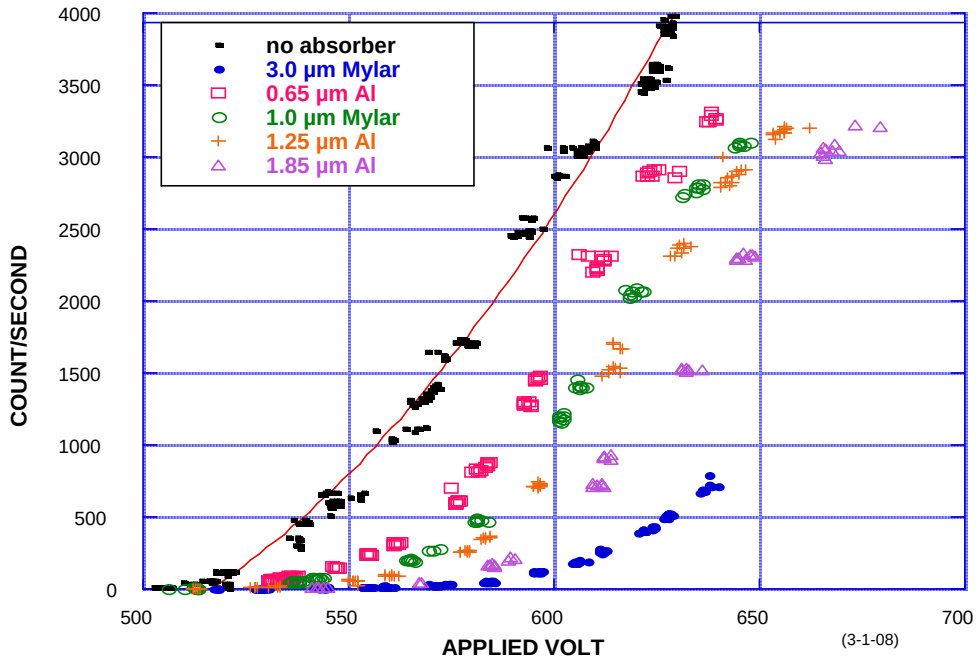

FIGURE 23. Effect of applied voltage on the counting rate measured when various absorbers are imposed.

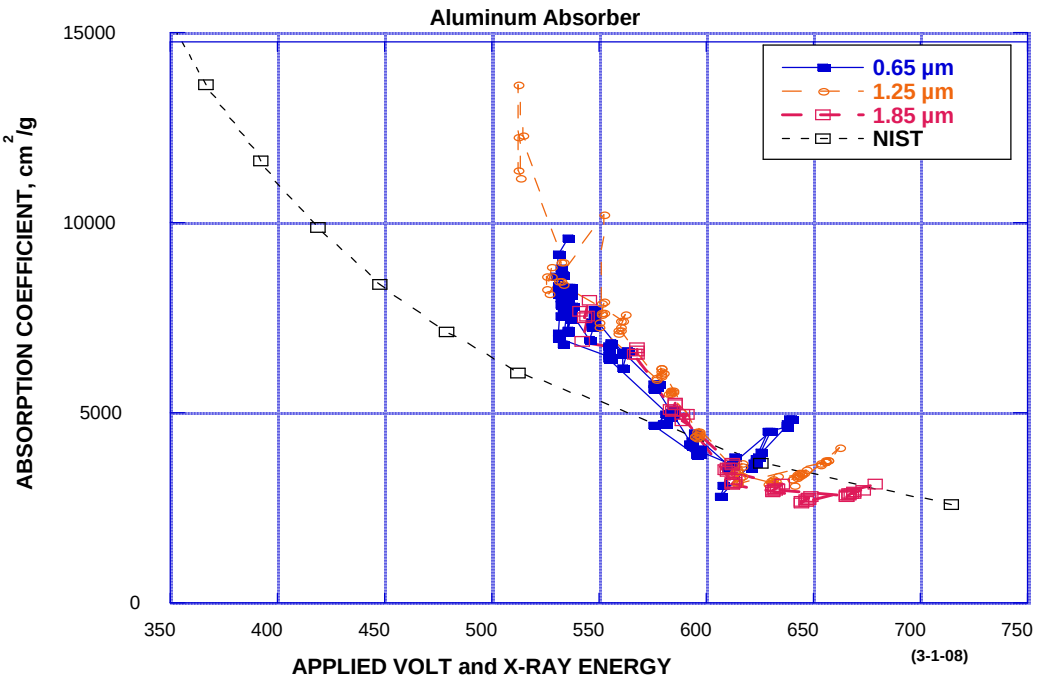

FIGURE 24. Comparison of absorption coefficients calculated using the aluminum absorbers and the tabulated values supplied by NIST for X-rays of the indicated energy.

The initial results suggested the radiation was energetic electrons. However, work done at Coolescence[31] indicated the radiation is X-rays because it is apparently not deflected by a magnetic field. To test this conclusion, a large magnet is used in an attempt to deflect the radiation, a picture of which is shown in Fig. 25. Radiation originating in the cell on the right, as described previously, passes through a beam defining slit, through 3 inches of magnetic field, and into a small-window GM tube (1.5 mm dia.) on the left. An applied field strength up to 10,000 G is measured with a Gauss meter. Although significant counting rates are observed, at no time is this rate changed by a magnetic field, as would be expected if the radiation had an electric charge.

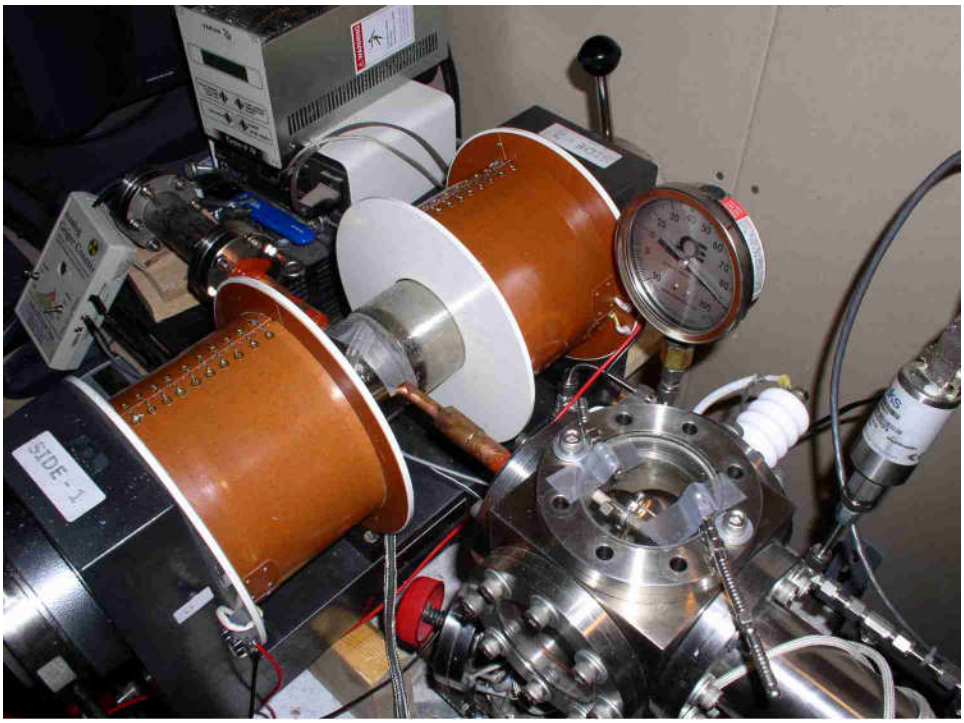

FIGURE 25. Picture of magnet used to deflect radiation from the gas discharge cell. The radiation is detected using a thin-window GM tube located at the left top.

IV. DISCUSSION

During gas discharge, X-radiation is always generated. In contrast, the particle radiation occurs infrequently, is often obscured by electrical noise generated by the discharge, and has a much lower flux compared to the X-ray emission. Nevertheless, both kinds of emission are sensitive to applied voltage and gas composition, which in each case cause changes in energy and intensity, but not to the same degree.

IV.1. Particle Emission

The intensity and characteristics of the spectrum is sensitive to composition of the gas, but less so to the basic material used as the cathode. The relationship between intensity and peak energy for the various energies is shown in Fig. 26 for different gas compositions. Apparently, addition of hydrogen causes the intensity of the various peaks to increase, thereby allowing the details of the spectrum to be more clearly seen in Fig. 12. The logarithmic behavior suggests that very large peaks might exist at an energy too low to be separated from the noise and much smaller peaks might exist at higher energies. As a result, only a small part of the full spectrum might be seen.

Each peak increases in energy as applied voltage is increased. This behavior can be seen in Fig. 27 where each peak at the same position in the spectrum is connected by a line. In general, the greater the energy of the emission, the greater the effect of applied voltage on its energy. When the gas contains only $D_2 + D_2O$ the intensity is too small to make the full spectrum visible. As a result, only the most intense peak is plotted and connected by a line. The observed effect of gas composition on energy and intensity encourages the belief that the peaks are produced by real emissions rather than by electrical noise.

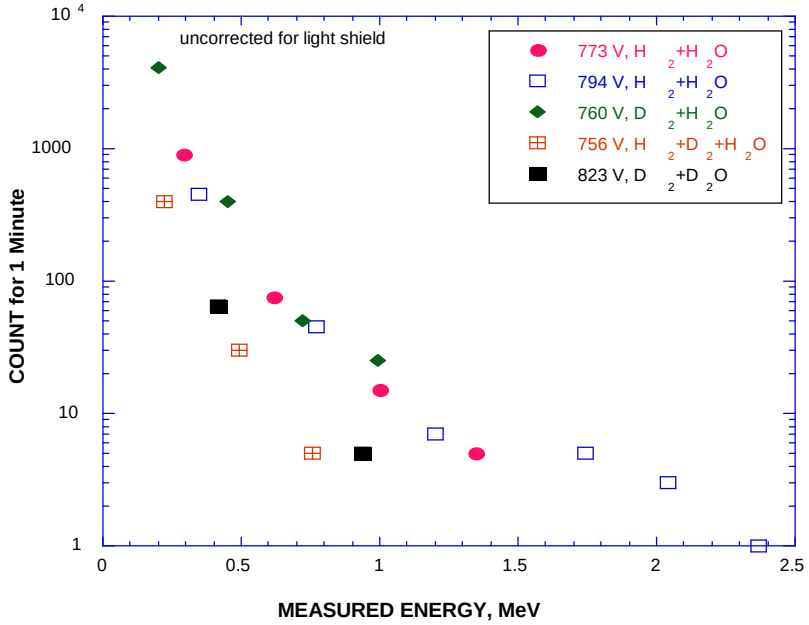

FIGURE 26. Effect of gas composition on the intensity of the various peaks.

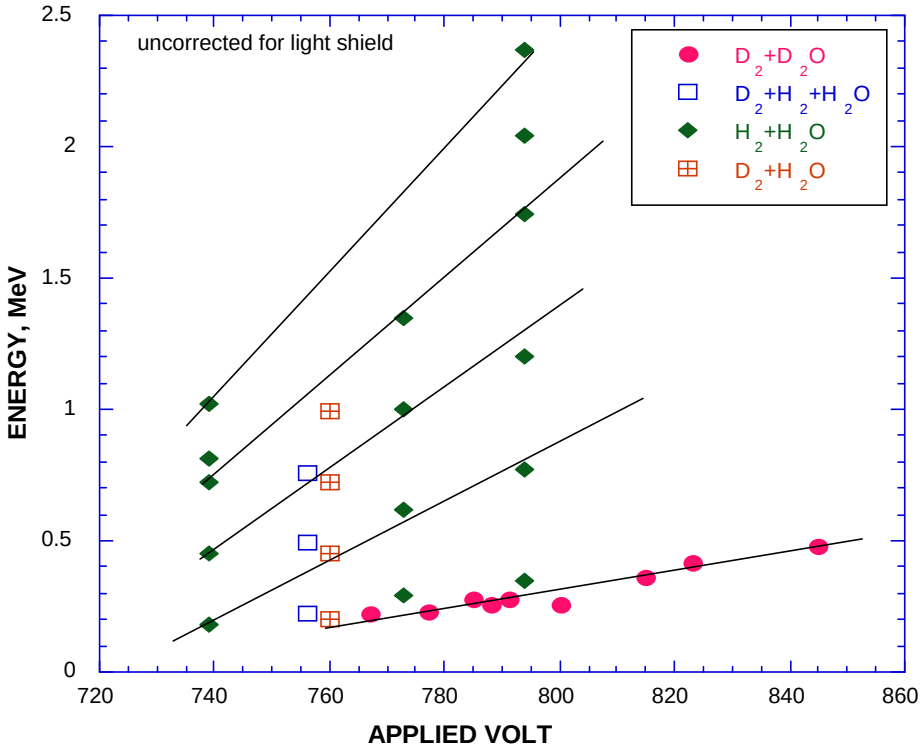

FIGURE 27. Effect of voltage on particle energy for various gas compositions and energy peaks. Lines are drawn between peaks of similar position in the spectrum.

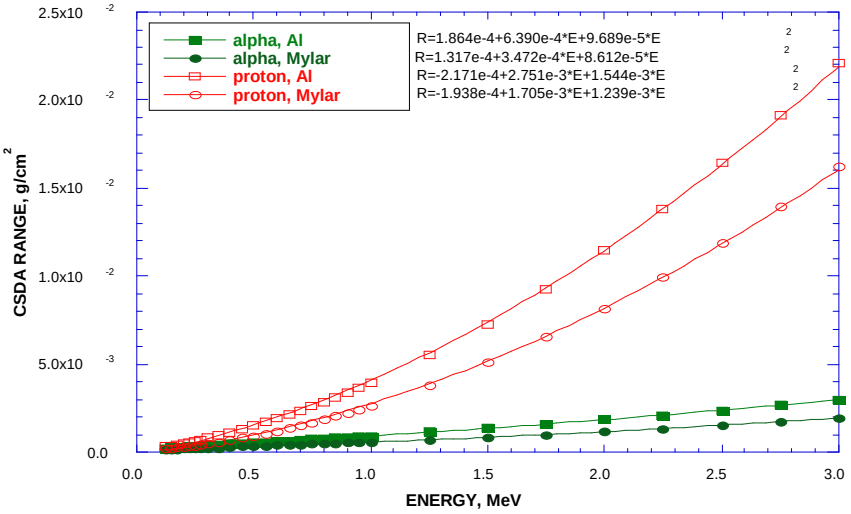

FIGURE 28. Range for alpha and proton in aluminum and Mylar from ASTAR.

What are the particles and what reaction causes their production? Because a light-shield is required, energy detected by the SBD needs to be corrected, depending on the kind of particle being measured. This requires the effect of this material be determined using published data from ASTAR. The effect of aluminum and Mylar are calculated from the data shown in Fig. 28 by dividing the slope at 1 MeV, an arbitrary energy near that of the particles, into the thickness density of the absorbers. The results are listed in Table 2. If the spectrum is produced by alpha particles, about 0.39 MeV must be added. If the particles are protons, addition of only 0.075 MeV is needed. The behavior of deuterons at this energy is very similar to that of protons. This information will now be used to identify the emission.

When a thin absorber is inserted, the energy of the particle is reduced without a significant reduction in intensity until an abrupt reduction is produced at the end of its range. Each kind of particle and absorbing material has a different behavior in this respect. Consequently, this behavior can be used to identify the radiation. For example, insertion of 3.0 μm Mylar (Fig. 10) shifts the peak designated 0.28 MeV off scale and moves the peak at 0.72 MeV to 0.34 MeV, a change of 0.38 MeV. Figure 13 shows a shift of 0.20 MeV when 3.0 μm Mylar is used in another study. The Mylar absorber has a density of 0.42 mg/cm^2, which would reduce an alpha energy by 0.81 MeV. Apparently, the particle is not an alpha. In contrast, a proton would lose 0.14 MeV. Again, this is not consistent with the measurement, although the discrepancy is in the direction expected to be produced by a deuteron or triton. However, if a triton is produced by fusion, a proton having about 3 MeV should also be emitted, which is not detected. Consequently, while the data cannot be fit exactly by the behavior of a known particle, the most likely particle is a deuteron. The conflict between the expected behavior of deuterons and the measurements can be attributed to errors in the ASTAR data in this energy range, to an error in the expected thickness of the Mylar absorber, and to errors resulting from the detection of a very small number of particles. Nevertheless, alpha emission of any energy is ruled out by these studies. In addition, the measured energy is much greater than would be expected from a chemical reaction or as a result of normal processes occurring in the discharge.

How can these results be explained? The work of Iwamura et al. [32] has shown that clusters of deuterons are involved in LENR reactions. Takahashi[33,34] has explored how they

might be made and proposed that members of the cluster carry away part of the energy. This conclusion follows if the cluster configuration is bound together tight enough to enter into a nuclear reaction as a unit. For such a nuclear reaction to occur, the unreacted members would have to be close enough to share in the energy released from the resulting reaction. In other words, the members of the cluster not actually involved in the nuclear reaction would carry away the energy resulting from a reaction between two of its members, as proposed by Takahashi. This work carries the idea further by finding that the energy is much lower than would be the case if the cluster had only a few members as proposed by Takahashi. Instead, the clusters appear to be large. For example, this work indicates that a cluster would have to contain nearly 20 deuterons for each to have an energy resulting from a fusion reaction near that found in this study. Because the clusters can have a variety of sizes, the resulting energy of deuterons emitted from a sample can have a variety of energies, but with a fixed relationship as is observed. In other words, each peak results from a cluster of a different size being the source of the nuclear reaction. Based on the intensity of the various observed energies, larger clusters appear to be more common than smaller ones with a distribution that is sensitive to the voltage applied to the discharge and to the gas composition. Apparently protium enhances this process without sharing the energy. If this mechanism and observations are correct, a search for emitted particles from the LENR process should focus on deuterons as the emitted particle with an energy between 0.5 and 3 MeV.

IV.2. Gas Loading

What appears to be anomalous radiation using a mixed oxide turns out to be radiation produced by potassium contamination. Nevertheless, this experience demonstrates the ability of the detector to find low-energy, low-intensity radiation. Further studies are underway.

Besides being a possible source of LENR, oxides containing finely divided palladium can absorb hydrogen in three ways. Before the hydrogen content can be related to the behavior or to theory, these three forms of hydrogen need to be determined separately. A preliminary study was done by determining the amount of deuterium that a sample takes up as a function of palladium content, as listed in Table 3. Although the data show significant scatter, some important patterns immerge. SiO_2 containing no Pd absorbed 0.09 wt % D_2, presumably as D_2 molecules. When a small amount of Pd (0.23%) was present, the amount of D_2 absorbed was less, but equally small. However, presence of 0.92% and 1.37% Pd caused a significant but similar increase in D_2 absorption. Although the Pd is present as very small particles, the average D/Pd ratio of about 12 is much greater than has been reported for similar particle size in the absence of a supporting oxide[35]. Even palladium nanoparticles grown in zeolite only reach a composition near D/Pd=2.[36]. A possible explanation for the unusually large amount of deuterium in the samples is that significant D+ is being retained by the oxide surface in addition to that being held by the Pd particles, as has been proposed previously.[37] Although this study is not complete, it shows evidence for the presence of the three kinds of D when Pd is mixed with an oxide. Similar studies need to be made for all such Pd-oxide combinations before any conclusions about the role of D in the fusion reaction can be determined in such materials. The enthalpy of reaction with D_2 will also be modified from that expected for pure Pd by these additional reactions.

IV.3. X-radiation

As can be seen in Fig. 24, the average energy of the X-rays emitted at 600 V is nearly equal to 600 eV. As applied voltage is reduced, the average energy of the X-rays is also reduced

and becomes less than applied voltage. This change could result because as applied voltage is lowered, more of the smaller X-ray energy is removed by the window of the GM resulting in a smaller average. Nevertheless, the average energy is nearly equal to applied voltage. Because energy of the X-rays changes with applied voltage, this radiation cannot result directly from k-radiation because this emission has a fixed value. Even when oxygen, with a k-transition at 525 eV, and nitrogen, with a value of 392 eV, are largely absent, the typical X-radiation is still produced. If the X-radiation resulted from interaction between ions and/or electrons with the gas, the intensity would be sensitive to gas pressure, which it is not. If the radiation results from Bremsstrahlung, bombardment of the cathode by ions appears to be the only other possibility. The process is enhanced by the presence of oxygen in the gas.

V. CONCLUSION

Anomalous radiation is produced when a glow discharge is produced in deuterium gas. This discharge consists of low-energy X-radiation and occasional energetic particles.

The energy of the X-radiation increases as voltage applied to the discharged is increased, with an energy equal to applied voltage at 600 V. Intensity increases with applied voltage and with increase in O/D ratio. The source does not appear to be k-radiation from oxygen or nitrogen. The intensity of X-radiation is at least 1000 times greater than the particle flux.

Insertion of Mylar absorbers suggests the particles are deuterons with energy peaks having various values between 0.5 and 3 MeV. The energy is sensitive to voltage applied to the cell and to gas composition.

Samples consisting of Pd mixed with various oxides absorb hydrogen in three different ways. Therefore, all hydrogen in such mixtures cannot be assumed to have reacted only with the Pd.

When radiation is measured from such mixtures, the amount of potassium needs to be low to avoid radiation from K^{40}.

References

1. Bush, B. F., Lagowski, J. J., Miles, M. H., and Ostrom, G. S., Helium production during the electrolysis of D_2O in cold fusion experiments, *J. Electroanal. Chem.* 304, 271, 1991.
2. Miles, M., Bush, B. F., Ostrom, G. S., and Lagowski, J. J., Heat and helium production in cold fusion experiments, in *Second Annual Conference on Cold Fusion, "The Science of Cold Fusion"*, Bressani, T., Giudice, E. D., andPreparata, G. Societa Italiana di Fisica, Bologna, Italy, Como, Italy, 1991, pp. 363.
3. Miles, M. and Bush, B. F., Search for anomalous effects involving excess power and helium during D_2O electrolysis using palladium cathodes, in *Third International Conference on Cold Fusion, "Frontiers of Cold Fusion"*, Ikegami, H. Universal Academy Press, Inc., Tokyo, Japan, Nagoya Japan, 1992, pp. 189.
4. Gozzi, D., Caputo, R., Cignini, P. L., Tomellini, M., Gigli, G., Balducci, G., Cisbani, E., Frullani, S., Garibaldi, F., Jodice, M., and Urciuoli, G. M., Helium-4 quantitative measurements in the gas phase of cold fusion electrochemical cells, in *Fourth International Conference on Cold*

Fusion, Passell, T. O. Electric Power Research Institute 3412 Hillview Ave., Palo Alto, CA 94304, Lahaina, Maui, 1993, pp. 6.
5. Miles, M. H. and Bush, B. F., Heat and helium measurements in deuterated palladium, in *Fourth International Conference on Cold Fusion*, Passell, T. O. Electric Power Research Institute 3412 Hillview Ave., Palo Alto, CA 94304, Lahaina, Maui, 1993, pp. 6.
6. Miles, M. H. and Bush, B. F., Heat and helium measurements in deuterated palladium, *Trans. Fusion Technol.* 26 (#4T), 156, 1994.
7. Gozzi, D., Caputo, R., Cignini, P. L., Tomellini, M., Gigli, G., Balducci, G., Cisbani, E., Frullani, S., Garibaldi, F., Jodice, M., and Urciuoli, G. M., Quantitative measurements of helium-4 in the gas phase of Pd + D2O electrolysis, *J. Electroanal. Chem.* 380, 109, 1995.
8. Miles, M., Johnson, K. B., and Imam, M. A., Heat and helium measurements using palladium and palladium alloys in heavy water, in *Sixth International Conference on Cold Fusion, Progress in New Hydrogen Energy*, Okamoto, M. New Energy and Industrial Technology Development Organization, Tokyo Institute of Technology, Tokyo, Japan, Lake Toya, Hokkaido, Japan, 1996, pp. 20.
9. Arata, Y. and Zhang, C., Presence of helium ($^2He_4$, $^2He_3$) confirmed in deuterated Pd-black by the "vi-effect" in a "closed QMS" environment, *Proc. Japan. Acad. B* 73, 62, 1997.
10. McKubre, M. C. H., Tanzella, F. L., Tripodi, P., and Hagelstein, P. L., The emergence of a coherent explanation for anomalies observed in D/Pd and H/Pd system: evidence for ^{4}He and ^{3}He production, in *8th International Conference on Cold Fusion*, Scaramuzzi, F. Italian Physical Society, Bologna, Italy, Lerici (La Spezia), Italy, 2000, pp. 3.
11. De Ninno, A., Frattolillo, A., Rizzo, A., Del Giudice, E., and Preparata, G., Report No. RT/2002/41/FUS, 2002.
12. McKubre, M. C. H., Review of experimental measurements involving dd reactions, PowerPoint slides, in *Tenth International Conference on Cold Fusion*, Hagelstein, P. L. andChubb, S. R. World Scientific Publishing Co., Cambridge, MA, 2003.
13. Storms, E. and Talcott, C. L., Electrolytic tritium production, *Fusion Technol.* 17, 680, 1990.
14. Sánchez, C., Sevilla, J., Escarpizo, B., Fernández, F. J., and Canizares, J., Nuclear products detection during electrolysis of heavy water with titanium and platinum electrodes, *Solid State Commun.* 71, 1039, 1989.
15. Srinivasan, M., Shyam, A., Sankaranarayanan, T. K., Bajpai, M. B., Ramamurthy, H., Mukherjee, U. K., Krishnan, M. S., Nayar, M. G., and Naik, Y. P., Tritium and excess heat generation during electrolysis of aqueous solutions of alkali salts with nickel cathode, in *Third International Conference on Cold Fusion, "Frontiers of Cold Fusion"*, Ikegami, H. Universal Academy Press, Inc., Tokyo, Japan, Nagoya Japan, 1992, pp. 123.
16. Sankaranarayanan, T. K., Srinivasan, M., Bajpai, M. B., and Gupta, D. S., Investigation of low-level tritium generation in Ni-H2O electrolytic cells, *Fusion Technol.* 30, 349, 1996.
17. Romodanov, V. A., Savin, V., Elksnin, V., and Skuratnik, Y., Reproducibility of tritium generation from nuclear reactions in condensed matter, in *Fourth International Conference on Cold Fusion*, Passell, T. O. Electric Power Research Institute 3412 Hillview Ave., Palo Alto, CA 94304, Lahaina, Maui, 1993, pp. 15.
18. Claytor, T. N., Jackson, D. D., and Tuggle, D. G., Tritium production from a low voltage deuterium discharge of palladium and other metals, *J. New Energy* 1 (1), 111, 1996.
19. Celani, F., Spallone, A., Tripodi, P., and Nuvoli, A., Measurement of excess heat and tritium during self-biased pulsed electrolysis of Pd-D_2O, in *Third International Conference on Cold*

Fusion, "Frontiers of Cold Fusion", Ikegami, H. Universal Academy Press, Inc., Tokyo, Japan, Nagoya Japan, 1992, pp. 93.
[20.] Clarke, B. W., Oliver, B. M., McKubre, M. C. H., Tanzella, F. L., and Tripodi, P., Search for ^{3}He and ^{4}He in Arata-style palladium cathodes II: Evidence for tritium production, *Fusion Sci. & Technol.* 40, 152, 2001.
[21.] Chêne, J. and Brass, A. M., Tritium production during the cathodic discharge of deuterium on palladium, *J. Electroanal. Chem.* 280, 199, 1990.
[22.] Mosier-Boss, P. A., Szpak, S., Gordon, F. E., and Forsley, L. P. G., Use of CR-39 in Pd/D co-deposition experiments, *Eur. Phys. J. Appl. Phys.* 40, 293-303, 2007.
[23.] Roussetski, A. S., Lipson, A. G., Lyakhov, B. F., and Saunin, E. I., Correct identification of energetic alpha and proton tracks in experiments on CR-39 charged particle detection during hydrogen desorption from Pd/Pd:Hx heterostructure, in *Condensed Matter Nuclear Science, ICCF-12*, Takahashi, A., Ken-ichiro, O., andIwamura, Y. World Scientific, Yokohama, Japan, 2005, pp. 304.
[24.] Lipson, A. G., Miley, G., Roussetski, A. S., Lyakhov, B. F., and Saunin, E. I., Reproducible nuclear emissions from Pd/PdO:Dx heterostrucutre during controlled exothermic deuterium desorption, in *Condensed Matter Nuclear Science, ICCF-12*, Takahashi, A., Ken-ichiro, O., andIwamura, Y. World Scientific, Yokohama, Japan, 2005, pp. 293.
[25.] Roussetski, A. S., CR-39 track detectors in cold fusion experiments: Review and perspectives, in *11th International Conference on Cold Fusion*, Biberian, J.-P. World Scientific Co, Marseilles, France, 2004, pp. 274.
[26.] Oriani, R. A. and Fisher, J. C., Nuclear reactions produced in an operating electrolytic cell, in *11th International Conference on Cold Fusion*, Biberian, J.-P. World Scientific Co., Marseilles, France, 2004, pp. 295.
[27.] Storms, E. K. and Scanlan, B., Radiation produced by glow discharge in deuterium, in *8th International Workshop on Anomalies in Hydrogen / Deuterium Loaded Metals. 2007.* http://www.iscmns.org/catania07/index.htm, Catania, Sicily, 2007.
[28.] Storms, E. K. and Scanlan, B., Radiation produced by glow discharge in a deuterium containing gas (Part 2), in *American Physical Society*, New Orleans, 2008.
[29.] Arata, Y. and Zhang, Y.-C., The Establishment of Solid Nuclear Fusion Reactor, *J. High Temp. Soc.* 34 (2), 85, 2008.
[30.] Case, L. C., Catalytic fusion of deuterium into helium-4, in *The Seventh International Conference on Cold Fusion*, Jaeger, F. ENECO, Inc., Salt Lake City, UT, Vancouver, Canada, 1998, pp. 48.
[31.] Cantwell, R. and McConnell, M., Partial Replication of Storms/Scanlan Glow Discharge Radiation, private communication, 2008.
[32.] Iwamura, Y., Sakano, M., and Itoh, T., Elemental analysis of Pd complexes: effects of D_2 gas permeation, *Jpn. J. Appl. Phys. A* 41 (7), 4642, 2002.
[33.] Takahashi, A., Deuteron cluster fusion and ash, in *ASTI-5* www.iscmns.org/, Asti, Italy, 2004.
[34.] Takahashi, A., Mechanism of deuteron cluster fusion by EQPET model, in *Tenth International Conference on Cold Fusion*, Hagelstein, P. L. andChubb, S. R. World Scientific Publishing Co.g, Cambridge, MA, 2003, pp. 809.
[35.] Everett, D. H. and Sermon, P. A., Crystallite size effects in the palladium/hydrogen system: A simultaneous sorption and X-ray study, *Zeit. Phys. Chem. Neue Folge Bd.* 114 (S), 109, 1979.

[36.] Nishimiya, N., Kishi, T., Mizushima, T., Matsumoto, A., and Tsutsumi, K., Hyperstoichiometric hydrogen occlusion by palladium nanoparticles included in NaY zeolite, *J. Alloys and Compounds* 319, 312, 2001.
[37.] Sermon, P. A. and Bond, G. C., *J. Catal.* 24, 467, 1974.